

On the Square Speed of Sound in High-Energy Collisions: Range of Values and How to Understand It

Ting-Ting Duan^{1,a)}, Fu-Hu Liu^{1,b)}, Khusniddin K. Olimov^{2,3,c)}

¹*Institute of Theoretical Physics, State Key Laboratory of Quantum Optics Technologies and Devices & Collaborative Innovation Center of Extreme Optics, Shanxi University, Taiyuan 030006, China*

²*Laboratory of High Energy Physics, Physical-Technical Institute of Uzbekistan Academy of Sciences, Chingiz Aytmatov Str. 2b, Tashkent 100084, Uzbekistan*

³*Department of Natural Sciences, National University of Science and Technology MISIS (NUST MISIS), Almalyk Branch, Almalyk 110105, Uzbekistan*

Abstract: After reviewing the sound speeds in various forms and conditions of matter, we investigate the sound speed of hadronic matter that has decoupled from the hot and dense system formed during high-energy collisions. We comprehensively consider factors such as energy loss of the incident beam, rapidity shift of leading nucleons, and the Landau hydrodynamic model for hadron production. The sound speed is related to the width or standard deviation of the Gaussian rapidity distribution of hadrons. The extracted square speed of sound lies within a range from 0 to 1/3 in most cases. For scenarios exceeding this limit, we also provide an explanation.

Keywords: square speed of sound, energy loss, rapidity shift, Gaussian rapidity distribution

PACS numbers: 12.40.Ee, 13.85.Ni, 13.87.Ce

1. Introduction

In high-energy collisions, the hot and dense system generated in regions with violently compressed participant nucleons exhibits a wealth of characteristics. Quantities such as pressure, energy density, entropy density, temperature, volume, and others can be measured or extracted using appropriate methods. In addition to the equation of state, which defines the ratio between pressure and energy density, both sound speed (c_s) and square speed of sound (c_s^2) are important extractable quantities that contribute to our understanding of collision system evolution processes as well as accelerated expansion phenomena in cosmology. For hadronic matter resulting from decoupling within a hot and dense environment, c_s^2 can be determined by taking the partial derivative of pressure with respect to energy density at constant entropy density; alternative formulations may arise due to relationships among thermodynamic quantities [1].

a) 202312602001@email.sxu.edu.cn

b) Correspondence: fuhuliu@163.com; fuhuliu@sxu.edu.cn, ORCID ID 0000-0002-2261-6899

c) Correspondence: khkolimov@gmail.com; kh.olimov@uzsci.net, ORCID ID 0000-0002-1879-8458

The values for c_s^2 vary across different models and types of matter while maintaining similar definitions. Beyond just high-energy collision systems characterized by their hot and dense state, other forms and conditions—such as neutron stars [2, 3], dark matter [4], dark energy [5–7], magnetized nuclear matter [8], gas composed of closed strings [9], and adiabatic evolution in heavy fields [10]—exhibit significant differences in their respective ranges for c_s^2 . Qualitative discussions on the various ranges of c_s^2 in different forms and conditions of matter are essential for enhancing our understanding of the ranges of c_s^2 associated with hadronic matter decoupled from hot and dense system.

Within neutron stars, a quantitative Bayes factor analysis indicates that the conformal bound $0 \leq c_s^2 \leq 1/3$ is violated [3], despite applying the same definition of c_s^2 as used for hadronic matter. As energy density increases, c_s^2 initially rises before exhibiting fluctuations—either large or small [2, 3]. The range of c_s^2 for neutron stars is found to be $0 \leq c_s^2 \leq 1$. For dark matter sound speed constrained by galactic scales, cases involving modified and extended Chaplygin gas yield values such that $0 \leq c_s^2 < 10^{-8}$ [4]. This value is indeed very small and presents a more competitive constraint compared to previous limits derived from anisotropic cosmic microwave background measurements and baryonic acoustic oscillations which exhibit power spectra.

Using a constant linear equation of state, the behavior of dark energy perturbations during radiation and matter epochs in both synchronous and conformal Newtonian gauges has been analytically studied in reference [5]. It was demonstrated that the range for sound speed can be constrained to $10^{-4} \leq c_s^2 \leq 1$, which contradicts results obtained from dark matter studies. Employing the Markov chain Monte Carlo method, a global analysis based on current observational data from anisotropic cosmic microwave background suggests that constraints on c_s^2 remain quite weak. Furthermore, if sound speed becomes negative, the system exhibits instability due to divergent classical perturbations [6]. Predictions across all scalar field models featuring standard kinetic terms indicate that $c_s^2 = 1$. However, models such as k -essence predict an effective sound speed significantly greater than one. Although it remains challenging to quantitatively measure the value of c_s^2 associated with dark energy directly, it can influence measurements related to other parameters [7].

Within the framework of the nonlinear Walecka model, a calculation for nuclear matter subjected to a background magnetic field at finite temperature and baryon chemical potential reveals that the presence of a magnetic field induces anisotropy in c_s^2 . Consequently, the parallel (or longitudinal) and perpendicular (or transverse) components, denoted as $c_s^{2(\parallel)}$ and $c_s^{2(\perp)}$, respectively, can exhibit variation [8]. Furthermore, related calculations indicate that $0 < c_s^2 < 1$ in nuclear matter at high baryon chemical potential, irrespective of whether a magnetic field is present or absent [8]. According to reference [9], matter in string gas cosmology can be conceptualized as a gas of closed strings, which suggests that $0 < c_s^2 \ll 1$. In accordance with the framework of adiabatic evolution in heavy fields [10], c_s^2 can be

expressed in terms of the effective mass of heavy fields and the turning rate of the background trajectory within multi-field space. This leads to a suppressed sound speed characterized by $0 < c_s^2 \ll 1$.

From this introduction—which provides only select examples regarding sound speed—it is evident that values for c_s^2 span a wide range. Even within nuclear matter, one finds that $0 < c_s^2 < 1$. It is therefore intriguing to investigate c_s^2 further and constrain its range during high-energy collisions. In this paper, we study c_s^2 under conditions prevalent in high-energy collisions based on energy loss from incident beams, rapidity shifts observed in leading nucleons, and utilizing Landau hydrodynamic model for hadron production. We elucidate its significance according to its defined ranges.

The remainder of this mini-review article is organized as follows: Section 2 gives formula description of square speed of sound; Section 3 presents possible range of square speed of sound and related explanation; finally, Section 4 provides a summary.

2. Formula description of square speed of sound

Let us denote by $E_{T\text{beam}}$, $E_{P\text{beam}}$, and m_N the energy of the target beam, energy of the projectile beam, and mass of protons, respectively. During collisions, we assume an energy loss rate denoted by k for either incident target or projectile nucleons. Following these collisions, we can express both energy (E_{LT}) and momentum (p_{LT}) for leading target nucleons alongside their counterparts—energy (E_{LP}) and momentum (p_{LP})—for leading projectile nucleons through

$$E_{LT} = (1 - k)E_{T\text{beam}}, \quad (1)$$

$$p_{LT} = \sqrt{E_{LT}^2 - m_N^2}, \quad (2)$$

$$E_{LP} = (1 - k)E_{P\text{beam}}, \quad (3)$$

and

$$p_{LP} = \sqrt{E_{LP}^2 - m_N^2}, \quad (4)$$

respectively. For the same size of target and projectile, one has

$$E_{T\text{beam}} = E_{P\text{beam}} = \frac{\sqrt{s_{NN}}}{2}, \quad (5)$$

where $\sqrt{s_{NN}}$ denotes the center-of-mass energy per nucleon pair.

For the leading nucleon, its transverse momentum is nearly zero, while its longitudinal momentum is approximately equal to its total momentum. In comparison with mid-rapidity, typically defined by $y_C = 0$, the rapidity shifts of the leading target and projectile nucleons are denoted as

$$y_{LT} \approx -\frac{1}{2} \ln \left(\frac{E_{LT} + p_{LT}}{E_{LT} - p_{LT}} \right) \quad (6)$$

and

$$y_{LP} \approx \frac{1}{2} \ln \left(\frac{E_{LP} + p_{LP}}{E_{LP} - p_{LP}} \right) \quad (7)$$

respectively. The total rapidity shift from the leading target nucleon to leading projectile nucleon can be given by

$$L = y_{LP} - y_{LT} \approx \frac{1}{2} \ln \left[\left(\frac{E_{LT} + p_{LT}}{E_{LT} - p_{LT}} \right) \left(\frac{E_{LP} + p_{LP}}{E_{LP} - p_{LP}} \right) \right]. \quad (8)$$

The total rapidity shift represents the distribution range of particles in one-dimensional rapidity y space. According to the Landau hydrodynamic model for hadron production in high-energy collisions [11–14], y follows an approximate Gaussian distribution characterized by a width or standard deviation σ [14, 15]. Based on properties of Gaussian distributions, it can be expected that approximately 99.7% of particles will fall within the rapidity range of $[-3\sigma, 3\sigma]$. If one considers a range of 6σ as representing the total rapidity shift L , then one has

$$\sigma \approx \frac{1}{6} L. \quad (9)$$

The Landau hydrodynamic model for hadron production results in the relationship between σ and c_s^2 to be [11, 16–21]

$$\sigma = \sqrt{\frac{8}{3} \frac{c_s^2}{1 - c_s^4} \ln \left(\frac{\sqrt{S_{NN}}}{2m_N} \right)}. \quad (10)$$

Then, the square speed of sound is expressed by

$$c_s^2 = \frac{1}{3\sigma^2} \left[-4 \ln \left(\frac{\sqrt{S_{NN}}}{2m_N} \right) + \sqrt{16 \ln^2 \left(\frac{\sqrt{S_{NN}}}{2m_N} \right) + 9\sigma^4} \right] \quad (11)$$

or

$$c_s^2 = -\frac{4}{3\sigma^2} \ln \left(\frac{\sqrt{S_{NN}}}{2m_N} \right) + \sqrt{\left[\frac{4}{3\sigma^2} \ln \left(\frac{\sqrt{S_{NN}}}{2m_N} \right) \right]^2 + 1}. \quad (12)$$

It is important to note that an analytical solution for non-conformal and viscous Landau hydrodynamics has been presented, along with a proposed form of the speed of sound in ref. [22]. This proposed solution can be generalized to ideal and conformal cases when appropriate limits are applied. Furthermore, this solution successfully describes the rapidity spectra observed in existing experimental data and offers a novel approach for probing the equation of state as well as extracting the speed of sound during heavy ion collisions. In ref. [22], another general relationship between σ^2 and c_s^2 can also be found. When compared to conformal solutions [11, 16–21], the non-conformal solution exhibits a slightly lower peak and a marginally larger σ^2 in rapidity distribution.

3. Possible range of square speed of sound and related explanation

Building upon these discussions, one can conveniently study the relationships between L and $\sqrt{s_{NN}}$, as well as between c_s^2 and $\sqrt{s_{NN}}$. To determine L , value for parameter k is required. In proton-proton collisions, the binary (nucleon-nucleon) collision number (ν) naturally equals 1. However, in proton-nucleus and nucleus-nucleus collisions, the maximum binary collision number (ν_{\max}) associated with a specific incident nucleon significantly exceeds 1. For instance, in proton-aluminum, proton-copper, and proton-uranium collisions where events exhibit maximum binary collision numbers of 9, 12, and 16 respectively; these correspond to fractions in their respective ν distributions being approximately 0.004%, 0.002%, and 0.010% [23]. Conversely, for these three specific types of collisions at $\nu = 1$, corresponding fractions are found to be about 47.177%, 34.479%, and 23.000%. It is evident that from $\nu = 1$ to $\nu = \nu_{\max}$, there is a significant decrease in corresponding fractions.

Some investigations indicate that, in multiple binary collisions, at least one instance experiences an energy loss of 50%, while the remaining instances incur an energy loss ranging from 10% to 25% [23–26]. To conduct a comprehensive study, it is advisable to consider as many values as possible within the range of $0.5 < k < 1$. The dependence of L on $\sqrt{s_{NN}}$ is illustrated in Figure 1. For comparison purposes, we set k values at 0.5, 0.6, 0.7, 0.8, and 0.9; these correspond to various curves marked with different colors in the panel. It is evident that L increases significantly with rising $\sqrt{s_{NN}}$ for all selected k values. Additionally, in the initial region of $\sqrt{s_{NN}}$, L exhibits a linear increase with respect to $\ln\sqrt{s_{NN}}$. Naturally, smaller k values result in larger L .

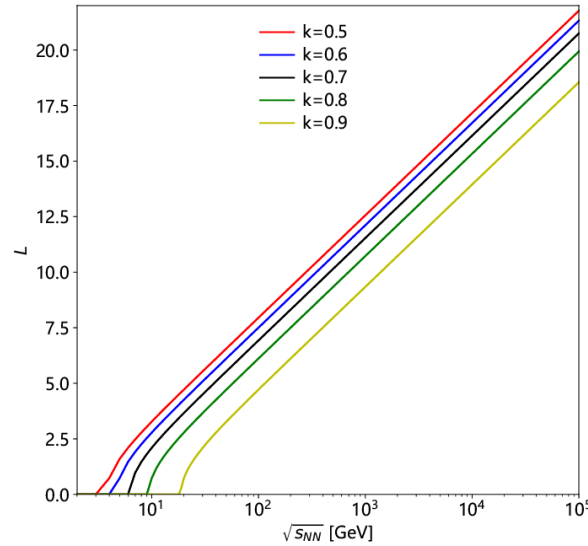


Fig. 1. Dependence of L on $\sqrt{s_{NN}}$, in which $k = 0.5, 0.6, 0.7, 0.8,$ and 0.9 which corresponds to various curves with different colors marked in the panel.

Figure 2 presents the relationship between c_s^2 and $\sqrt{s_{NN}}$ at $\sigma = L/6$, which reflects the required and reasonable correlation between σ and L . For comparative analysis, we again utilize k values of 0.5, 0.6, 0.7, 0.8, and 0.9 corresponding to distinct curves represented by

different colors within the panel. The results demonstrate that c_s^2 increases markedly with increasing $\sqrt{s_{NN}}$ across various k values; however, in some cases—specifically above hundreds of GeV—the growth rate of c_s^2 begins to gradually decelerate, where smaller k leadings to larger c_s^2 outcomes; notably many calculated c_s^2 remain below $1/3$. Only when $\sqrt{s_{NN}}$ exceeds approximately ten TeV do some instances yield c_s^2 greater than $1/3$.

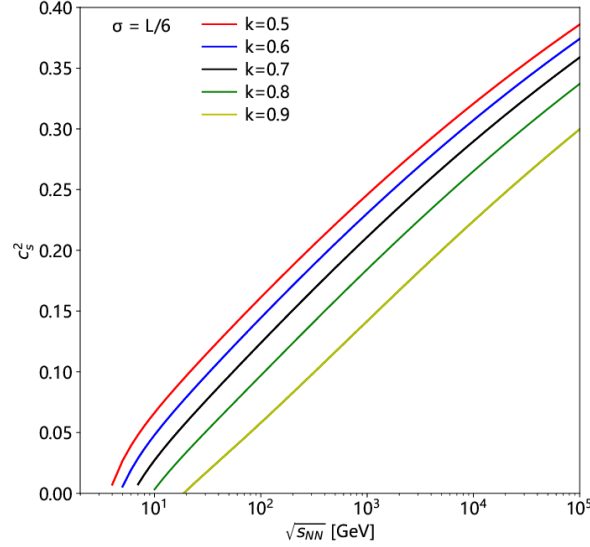


Fig. 2. Dependence of c_s^2 on $\sqrt{s_{NN}}$ at $\sigma = L/6$, in which $k = 0.5, 0.6, 0.7, 0.8,$ and 0.9 which corresponds to various curves with different colors marked in the panel.

The dependence of c_s^2 on $\sqrt{s_{NN}}$ is illustrated in Figure 3 for different values of σ , specifically $\sigma = 0.2L$ (a), $0.4L$ (b), $0.6L$ (c), and $0.8L$ (d). In each panel, the parameter $k = 0.5, 0.6, 0.7, 0.8,$ and 0.9 , corresponding to various curves represented by different colors, is employed. Notably, all four values of σ used in Figure 3 are greater than the value of $\sigma = L/6$ utilized in Figure 2; however, it should be noted that $\sigma = 0.2L$ is closest to this reference point. In all cases examined, there is a significant increase in c_s^2 with rising values of $\sqrt{s_{NN}}$. Furthermore, at energies exceeding hundreds of GeV—even down to approximately ten GeV—the growth rate of c_s^2 begins to decelerate gradually. It is evident that while $c_s^2 > 1/3$ holds true for most scenarios considered here, it remains less than one throughout the analysis presented in Figure 3; however, it must be emphasized that the values depicted are not physically realizable under standard conditions but serve primarily as a means to explore broader trends when parameters exceed physical limits.

Although the relationships between σ and L shown in Figure 3 may lack physical justification, the mathematical dependence of c_s^2 on $\sqrt{s_{NN}}$ can still be derived analytically. This study proposes a reasonable relationship: namely, $\sigma = L/6$, which establishes a connection between Gaussian distribution width σ and rapidity shift L . If rapidity does not conform to Gaussian distribution at very high energies (e.g., above several hundred GeV), yet adheres instead to a superposition model comprising two or three Gaussian distributions, then

one would identify two or three emission sources along with their respective widths σ and square speed of sound c_s^2 . Although each c_s^2 can be obtained from the relationship with σ [Eqs. (10)-(12)], each σ can no longer be obtained from the relationship with L [Eq. (9)].

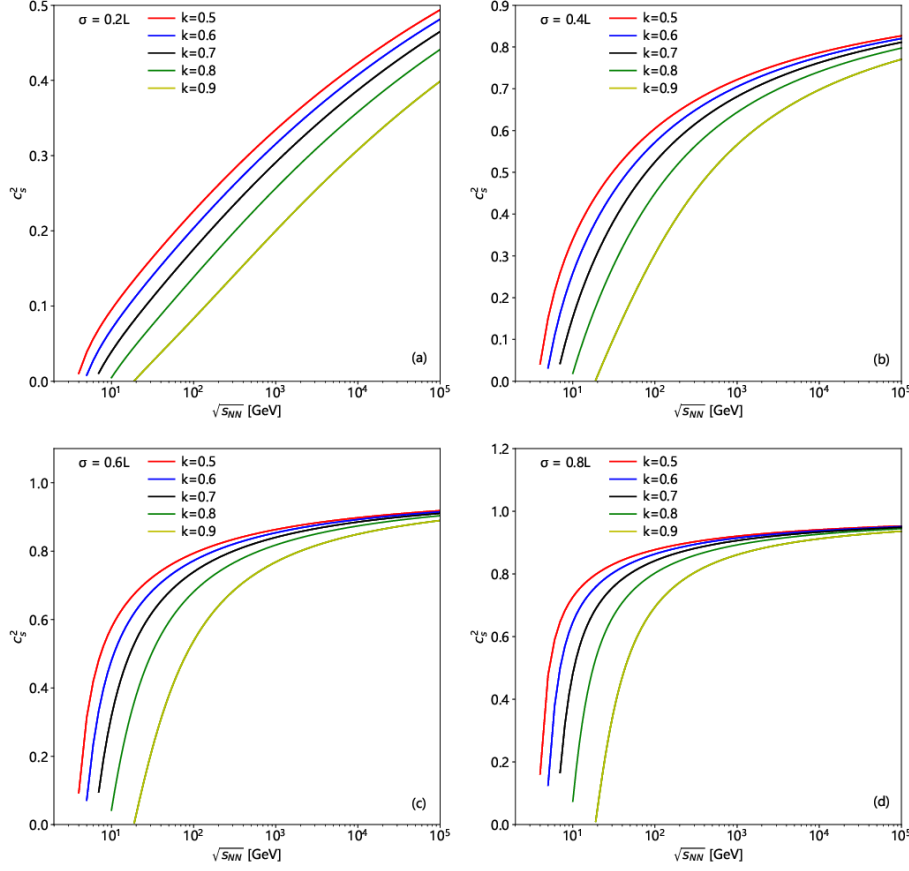


Fig. 3. Dependence of c_s^2 on $\sqrt{s_{NN}}$ at different σ , where $\sigma = 0.2L$ (a), $0.4L$ (b), $0.6L$ (c), and $0.8L$ (d), respectively. In each panel, $k = 0.5, 0.6, 0.7, 0.8,$ and 0.9 which corresponds to various curves with different colors.

When two Gaussian distributions are required, they may be interpreted as contributions from target and projectile sources respectively. Conversely, if three distributions are necessary, these could correspondingly represent contributions from target, central, and projectile sources where ideally the contribution from the central source should dominate. This approach yields maximal values for c_s^2 , in relation to central source while resulting in lower values for both target and projectile sources. At the energy levels currently achievable in laboratories, three Gaussian distributions are sufficient, and there appears to be no necessity for a fourth.

Regardless of the relationship between c_s^2 and L , there exist explanations regarding the magnitude of c_s^2 . Let d denote the spatial dimension; it is established that $c_s^2 = 1/d$ for matter produced in high-energy collisions [27, 28], irrespective of whether this matter exhibits liquid-like or gas-like characteristics. It should be noted that the distinction between liquid-like and gas-like states is not sharply defined; however, particles in a liquid-like state typically have

a mean free path smaller than those in a gas-like state. For an ideal gas composed of massless particles with zero shear modulus in three-dimensional space, one finds that $c_s^2 = 1/3$ [29–38]. Generally speaking, for ideal gases containing massive particles, it holds that $c_s^2 < 1/3$.

In certain specific scenarios—such as when matter formed from non-central collisions resides within a thermalized cylinder aligned along the beam direction while exhibiting transverse flow without having expanded into other directions—or when considering matter situated within the reaction plane [39, 40]—it can be observed that $c_s^2 = 1/2$ for massless particles and $c_s^2 < 1/2$ for massive particles. Conversely, if matter generated from central collisions exists within such a thermalized cylinder without expansion beyond its boundaries, then one finds that $c_s^2 = 1$ for massless particles and $c_s^2 < 1$ for massive ones. Both cases where $c_s^2 < 1/2$ and where $c_s^2 < 1$ correspond to early hadron production.

As time progresses, the matter or thermalized cylinder resulting from non-central collisions expands into additional dimensions; this leads to a decrease in c_s^2 , reducing it from below 1/2 to below 1/3. Furthermore, as the matter or thermalized cylinder originating from central collisions also expands outwardly beyond its cylindrical confines, this results in an accelerated decline of c_s^2 from below 1 to below 1/3. In general terms, the particle measurements obtained through experiments pertain to final states which arise after sufficient expansion has occurred, corresponding to values of c_s^2 that fall beneath 1/3.

However, the situation becomes more complex when strongly coupled quark-gluon plasma (sQGP) is formed in central heavy ion collisions at high energy. The formation of sQGP leads to a longer duration of the central collision system, resulting in greater expansion and a lower c_s^2 compared to non-central collision systems. In our view, the extraction of c_s^2 is highly dependent on the assumed physical models. It is crucial to adopt a reasonable and reliable physical framework along with its model representation if one aims to extract an accurate value for c_s^2 . This work presents an alternative method for extracting c_s^2 .

In our previous study [39], based on the Landau hydrodynamic model [11–14, 15], we investigated c_s^2 in both central and non-central gold-gold (Au-Au) collisions at $\sqrt{s_{NN}} = 19.6, 62.4, 130, \text{ and } 200$ GeV, as well as in copper-copper (Cu-Cu) collisions at $\sqrt{s_{NN}} = 22.4, 62.4, \text{ and } 200$ GeV by analyzing pseudorapidity distributions of charged particles. Our findings indicated that c_s^2 in central collisions is slightly lower than that observed in non-central collisions; however, both values are approximately within the range from 1/3 to 1/2. When examining leading nucleons within the target and projectile regions, we found that c_s^2 drops significantly below 1/3 due to these nucleons being in a gas-like state. These results align with those from our other prior research [40], which focused on proton-proton (pp) [proton-antiproton (p \bar{p})] collisions at GeV and TeV energies. Both the works [39, 40] gave σ and c_s^2 each to each, then the connection between L and c_s^2 is established due to $L = 6\sigma$.

Before the summary, we would like to emphasize that the underlying physical reason for the relationship between c_s^2 and d can be attributed to varying number densities of matter. In

central collisions, a thermalized cylinder without additional expansion indicates a high particle number density, which should lead to a large value of c_s^2 . However, in scenarios involving sQGP, prolonged expansion significantly reduces both density and c_s^2 . Conversely, in non-central collisions, a thermalized cylinder exhibiting transverse flow but lacking other forms of expansion suggests an intermediate density, resulting in an intermediate value for c_s^2 . As the collision system undergoes sufficient evolution, there is a notable decrease in density that causes c_s^2 to diminish to comparatively small values. The values of c_s^2 extracted at fixed $\sqrt{s_{NN}}$, as obtained in this work, pertain to the final stage of system evolution.

4. Summary

The square speeds of sound in various forms and conditions of matter within the universe have been reviewed, with a particular focus on the square speed of sound in hadronic matter that decouples from hot and dense systems formed during high-energy collisions. This study comprehensively considers factors such as energy loss of the incident beam, rapidity shifts of leading nucleons, and the application of the Landau hydrodynamic model for hadron production. Notably, the square speed of sound is correlated with the width or standard deviation of the Gaussian rapidity distribution observed in hadron production.

The extracted values for the square speed of sound range from 0 to 1/3 in most cases. For scenarios where this value exceeds 1/3 but does not surpass 1/2, we interpret these results as indicative of non-central collisions. In such cases, hot and dense matter is generated within a thermalized cylinder aligned along the beam direction while exhibiting transverse flow; however, it has yet to expand in other directions. Conversely, when values exceed 1/2 but remain below 1, we attribute these findings to central collisions wherein hot and dense matter also forms within a thermalized cylinder oriented along the beam direction without having expanded beyond its cylindrical boundaries. Over time, these concerned values rapidly decline into range from 1/3 to 1/2 and even further down into range from 0 to 1/3 due to substantial system expansion.

Data Availability Statement

Data sharing not applicable to this article as no data sets were generated during the current study. The data used to support the findings of this study and some outcome or conclusive statements are included within the article and are cited at relevant places within the text as references.

Ethical Approval

The authors declare that they are in compliance with ethical standards regarding the content of this paper.

Conflicts of Interest

The authors declare that there are no conflicts of interest regarding the publication of this paper.

Acknowledgments

The work of Shanxi Group was supported by the National Natural Science Foundation of China under Grant No. 12147215. The work of K.K.O. was supported by the Agency of Innovative Development under the Ministry of Higher Education, Science and Innovations of the Republic of Uzbekistan within the fundamental project No. F3-20200929146 on analysis of open data on heavy-ion collisions at RHIC and LHC.

References

- [1] R. V. Gavai, S. Gupta, and S. Mukherjee, “The speed of sound and specific heat in the QCD plasma: hydrodynamics, fluctuations and conformal symmetry,” *Physical Review D*, vol. 71, article 074013, 2005.
- [2] T. Kojo, “QCD equations of state and speed of sound in neutron stars,” *AAPPS Bulletin*, vol. 31, p. 11, 2021.
- [3] L. Brandes, W. Weise, and N. Kaiser, “Inference of the sound speed and related properties of neutron stars,” *Physical Review D*, vol. 107, article 014011, 2023.
- [4] P. P. Avelino and V. M. C. Ferreira, “Constraints on the dark matter sound speed from galactic scales: the cases of the modified and extended Chaplygin gas,” *Physical Review D*, vol. 91, article 083508, 2015.
- [5] G. Ballesteros and J. Lesgourgues, “Dark energy with non-adiabatic sound speed: initial conditions and detectability,” *Journal of Cosmology and Astroparticle Physics*, vol. 2010, no. 10, p. 014, 2010.
- [6] J.-Q. Xia, Y.-F. Cai, T.-T. Qiu, G.-B. Zhao, and X. M. Zhang, “Constraints on the sound speed of dynamical dark energy,” *International Journal of Modern Physics D*, vol. 17, pp. 1229–1243, 2008.
- [7] S. Hannestad, “Constraints on the sound speed of dark energy,” *Physical Review D*, vol. 71, article 103519, 2005.
- [8] R. Mondal, N. Chaudhuri, P. Roy, and S. Sarkar, “Speed of sound in magnetized nuclear matter,” 2023, <https://arxiv.org/abs/2312.03310>.
- [9] N. Lashkari and R. H. Brandenberger, “Speed of sound in string gas cosmology,” *Journal of High Energy Physics*, vol. 2008, no. 09, p. 082, 2008.
- [10] A. Achúcarro, V. Atal, S. Céspedes, J.-O. Gong, G. A. Palma, and S. P. Patil, “Heavy fields, reduced speeds of sound and decoupling during inflation,” *Physical Review D*, vol. 86, article 121301(R), 2012.
- [11] L. D. Landau, “Multiple production of particles under collision of rapid particles” *Izvestiya Akademii Nauk: Series Fizicheskikh*, vol. 17, p. 51–67, 1953.

- [12] I. M. Khalatnikov, “Some questions of the relativistic hydrodynamics,” *Journal of Experimental and Theoretical Physics*, vol. 27, pp. 529–541, 1954.
- [13] S. Z. Belen’kji and L. D. Landau, “Hydrodynamic theory of multiple production of particles,” *Il Nuovo Cimento*, vol. 3, pp. 15–31, 1956.
- [14] P. A. Steinberg, “Bulk dynamics in heavy ion collisions,” *Nuclear Physics A*, vol. 752, pp. 423–432, 2005
- [15] Z. J. Jiang, H. P. Deng, Y. Zhang, and H. L. Zhang, “Unified descriptions of Hwa-Bjorken and Landau relativistic hydrodynamics and the pseudorapidity distributions in high energy heavy ion collisions,” *Nuclear Physics Review*, vol. 32, pp. 398–404, 2015.
- [16] C.-Y. Wong, “Landau hydrodynamics reexamined,” *Physical Review C*, vol. 78, article 054902, 2008.
- [17] E. V. Shuryak, “Multiparticle production in high energy particle collisions,” *Yadernaya Fizika*, vol. 16, pp. 395–405, 1972.
- [18] O. V. Zhironov and E. V. Shuryak, “Multiple production of hadrons and predictions of the Landau theory,” *Yadernaya Fizika*, vol. 21, pp. 861–867, 1975.
- [19] P. Carruthers and M. Duong-Van, “Rapidity and angular distributions of charged secondaries according to the hydrodynamical model of particle production,” *Physical Review D*, vol. 8, pp. 859–874, 1973.
- [20] P. Carruthers, “Heretical models of particle production,” *Annals of the New York Academy of Sciences*, vol. 229, pp. 91–123, 1974.
- [21] M. Gazdzickia, M. Gorensteinc, and P. Seybothe, “Onset of deconfinement in nucleus-nucleus collisions: review for pedestrians and experts,” *Acta Physica Polonica B*, vol. 42, pp. 307–352, 2011.
- [22] D. Biswas, K. Deka, A. Jaiswal, and S. Roy, “Viscosity, non-conformal equation of state and sound velocity in Landau hydrodynamics,” *Physical Review C*, vol. 102, article 014912, 2020.
- [23] B. Liu and Y. C. Wang, “Multiplicity distributions of produced particles and energy loss in proton-nucleus collisions at 200 GeV/c,” *High Energy Physics and Nuclear Physics* (successor *Chinese Physics C*), vol. 11, pp. 231–237, 1987.
- [24] J. Hüfner and A. Klar, “Nuclear stopping power for ultrarelativistic protons,” *Physics Letters B*, vol. 145, pp. 167–170, 1984.
- [25] S. Daté, M. Gyulassy, and H. Sumiyoshi, “Nuclear stopping power at high energies,” *Physical Review D*, vol. 32, pp. 619–636 (1985).
- [26] F.-H. Liu, “Transverse-energy distribution in proton–nucleus collisions at high energy,” *Canadian Journal of Physics*, vol. 79, pp. 739–748, 2001.
- [27] K.-Y. Kim and I. Zahed, “Baryonic response of dense holographic QCD,” *Journal of High Energy Physics*, vol. 2008, no. 12, p. 075, 2008
- [28] E. I. Buchbinder, A. Buchel, and S. E. Vázquez, “Sound waves in (2+1) dimensional

- holographic magnetic fluids,” *Journal of High Energy Physics*, vol. 2008, no. 12, p. 090, 2008.
- [29] A. Bazavov, T. Bhattacharya, C. DeTar et al., “The equation of state in (2+1)-flavor QCD,” *Physical Review D*, vol. 90, article 094503, 2014.
- [30] U. Heinz, P. Sorensen, A. Deshpande et al., “Exploring the properties of the phases of QCD matter – research opportunities and priorities for the next decade,” 2015, <https://arxiv.org/abs/1501.06477>.
- [31] B. Betz, “Jet propagation and Mach-cone formation in (3+1)-dimensional ideal hydrodynamics,” 2009, <https://arxiv.org/abs/0910.4114>, Ph.D. Thesis, University Frankfurt, Germany, 2009.
- [32] P. Castorina, J. Cleymans, D. E. Miller, and H. Satz, “The speed of sound in hadronic matter,” *The European Physical Journal C*, vol. 66, pp. 207–213, 2010.
- [33] V. Roy and A. K. Chaudhuri, “Equation of state dependence of Mach cone like structures in Au+Au collisions,” *Journal of Physics G*, vol. 37, article 035105, 2010.
- [34] A. Cherman and T. D. Cohen, “A bound on the speed of sound from holography,” *Physical Review D*, vol. 80, article 066003, 2009.
- [35] P. M. Hohler and M. A. Stephanov, “Holography and the speed of sound at high temperatures,” *Physical Review D*, vol. 80, article 066002, 2009.
- [36] C. P. Herzog and S. S. Pufu, “The second sound of SU(2),” *Journal of High Energy Physics*, vol. 2009, no. 04, p. 126, 2009.
- [37] S. K. Ghosh, T. K. Mukherjee, M. G. Mustafa, and R. Ray, “QGP susceptibilities from PNJL model,” *Indian Journal of Physics*, vol. 85, pp. 87–91, 2011.
- [38] U. Gürsoy, E. Kiritsis, L. Mazzanti, and F. Nitti, “Deconfinement and gluon plasma dynamics in improved holographic QCD,” *Physical Review Letters*, vol. 101, article 181601, 2008.
- [39] L.-N. Gao and F.-H. Liu, “On pseudorapidity distribution and speed of sound in high energy heavy ion collisions based on a new revised Landau hydrodynamic model,” *Advances in High Energy Physics*, vol. 2015, Article ID 184713, 23 pages, 2015.
- [40] L.-N. Gao and F.-H. Liu, “On distributions of emission sources and speed of sound in proton-proton (proton-antiproton) collisions,” *Advances in High Energy Physics*, vol. 2015, Article ID 641906, 10 pages, 2015.